g-Factor Measurements at RISING: The Case of ^{127}Sn

L. Atanasova[1], D. L. Balabanski[2,3], M. Hass[4], D. Bazzacco[5], F. Becker[6], P. Bednarczyk[6,7], G. Benzoni[8], N. Blasi[8], A. Blazhev[9], A. Bracco[8], C. Brandau[6,10], L. Caceres[6,11], F. Camera[8], S. K. Chamoli[4], F.C.L. Crespi[8], P. Detistov[1], P. Doornenbal[6], C. Fahlander[12], E. Farnea[5], G. Georgiev[13], J. Gerl[6], K. Gladnishki[3], M. Górska[6], H. Grawe[6], J. Grebosz[6,7], R. Hoischen[12], G. Ilie[9,14], M. Ionescu-Bujor14, A. Iordachescu[14], A. Jungclaus[11], G. Lo Bianco[3], M. Kmiecik[7], I. Kojouharov[6], N. Kurz[6], S. Lakshmi[4], R. Lozeva[1,15], A. Maj[7], D. Montanari[8], G. Neyens[15], M. Pfützner[16], S. Pietri[10], Zs. Podolyák[10], W. Prokopowicz[6,7], D. Rudolph[12], G. Rusev[17], T. R. Saito[6], A. Saltarelli[3], H. Schaffner[6], R. Schwengner[17], G. Simpson[18], S. Tashenov[6], J. J. Valiente-Dobón[19], N. Vermeulen[15], J. Walker[6,10], E. Werner-Malento[6,16], O. Wieland[8], and H. J. Wollersheim[6]

[1] Faculty of Physics, University of Sofia, BG-1164 Sofia, Bulgaria
[2] INRNE, Bulgarian Academy of Sciences, BG-1784 Sofia, Bulgaria
[3] Universitá di Camerino and INFN-Perugia, 62032 Camerino, Italy
[4] Weizmann Institute of Science, Rehovot 76100, Israel
[5] Universitá di Padova and INFN-Padova, 35131 Padova, Italy
[6] GSI, Planckstrasse 1, D-64291, Darmstadt, Germany
[7] IFJ PAN, Polish Academy of Sciences, PL-31-342 Kraków, Poland
[8] Universitá di Milano and INFN-Milano, 20133 Milano, Italy
[9] IKP, Universität zu Köln, D-50937, Köln, Germany
[10] Department of Physics, University of Surrey, Guildford, GU2 7XH, UK
[11] Universidad Autonoma de Madrid, E-28049 Madrid, Spain
[12] Department of Physics, Lund University, S-22100 Lund, Sweden
[13] CSNSM, F-91405 Orsay Campus, France
[14] NIPNE, RO-077125, Bucharest, Romania
[15] IKS, K.U.Leuven, 3001 Leuven, Belgium
[16] IEP, Warsaw University, PL-00-681 Warsaw, Poland
[17] Institut für Strahlenphysik, FZ Rossendorf, D-01314, Dresden, Germany
[18] LPSC, 38026 Grenoble Cedex, France
[19] INFN - Laboratori Nazionali di Legnaro, 35020 Legnaro (Padova), Italy

Abstract. We report a g-factor measurement of the $19/2^+$ $T_{1/2} = 4.5(3)$ μs isomer in ^{127}Sn, which was carried out within the g-RISING project at GSI, Darmstadt, Germany, utilizing the time-differential perturbed angular distribution method. Isomers in $A \approx 130$ nuclei were populated in relativistic projectile fragmentation of a ^{136}Xe beam at $E/A = 600$ MeV on a 1024 mg/cm^2 Be production target. Fully-stripped ions were separated with the fragment separator, which allowed the preservation of the orientation of the nuclear spin ensemble as obtained in the reaction. The ions were implanted in a Copper plate, which provided a perturbation-free environment for the isomeric γ decay. The nuclei of interest were tracked and identified on an event-by-event basis and ion-γ coincidences were recorded.

The γ rays deexciting the isomers were detected with eight Cluster Ge detectors mounted in the horizontal plane perpendicular to a 0.12 T external magnetic field. The experiment, data analysis and preliminary results are presented.

1 Introduction

The g-RISING experimental campaign was carried out at the GSI laboratory in Darmstadt, Germany within a RISING (Rare ISotope INvestigations at GSI) project [1] and aimed at g factors studies of isomers in exotic nuclei far from stability which were populated in projectile fragmentation or fission at relativistic energies. Isomers have a rather pure single particle configuration in regions around doubly-magic nuclei. Measurements of their g factors can provide information about their wave functions and their purity. They can confirm suggested spin and parity assignments, especially in regions far from stability, where they are based on theoretical predictions or analogy with neighbouring nuclei.

Three experiments were approved for the g-RISING campaign. Two of them aimed at studies of isomeric g factors in the vicinity of the doubly-magic ^{132}Sn. The isomers of interest were populated in the fragmentation of a ^{136}Xe beam in the first case, and in relativistic fission of the ^{238}U in the second. This makes possible the direct comparison of the spin-alignment in fragmentation and fission reactions at relativistic energies and provides two independent measurements of the g factor of the $(19/2^+)$, $T_{1/2} = 4.5(3)$ μs isomer in ^{127}Sn [2]. Here we report the status of the analysis of the fragmentation experiment.

The configurations of the isomeric states in Sn isotopes below the N = 82 shell gap consist of neutron holes in the $d_{3/2}$, $h_{11/2}$ and $s_{1/2}$ shell model orbits. The corresponding empirical g factors of these states, which are based on measurements of states ascribed to single-particle configurations, are $g(d_{3/2}) \approx 0.50$, $g(h_{11/2}) \approx -0.24$ and $g(s_{1/2}) \approx -2.1$. For non-pure shell model states, the g factor depends also on the configuration mixing.

Microsecond $19/2^+$ isomers were observed in the odd-A Sn isotopes with masses between $A = 119$ and $A = 129$ [3]. The spin and parity assignments for the isomer in ^{127}Sn are based on energy systematic and comparison with theoretical calculations. The excitation energies of the $19/2^+$ states are similar to those of the 5^- isomers in the neighbouring even-even Sn isotopes. Thus, it was suggested [2] that the main component of the wave function of the isomeric level is $(\nu h^{-1}_{11/2} \otimes 5^-)_{19/2+}$. The measured g-factor of the 5^- isomers is $g \approx -0.067(13)$ [4] which suggests that the major contribution in the 5^- wave function is due to the $(\nu s^{-1}_{1/2} h^{-1}_{11/2})$ configuration, which has an empirical g factor of $g(s_{1/2}h_{11/2}) \approx -0.093$.

The $19/2^+$ isomers are suggested to decay partially via strongly hindered transitions of predominantly M2 character to a $15/2^-$ state in $^{123-127}$Sn. This state, together with the $11/2^-$ and $13/2^-$ states are expected to be rather pure members of the $h_{11/2}$ multiplet. Because of *L* forbidenness, this transition cannot take

place between states with the $(\nu h_{11/2}^{-3})$ and $(\nu s_{1/2}^{-1} h_{11/2}^{-2})$ configurations and an admixture of $(\nu g_{7/2}^{-1} h_{11/2}^{-2})$ is suggested in the $(19/2^+)$ wave function [2]. Different g factors are expected for these two configurations: $g(s_{1/2}^{-1} h_{11/2}^{-2}) \approx -0.156$ and $g(g_{7/2}^{-1} h_{11/2}^{-2}) \approx -0.23$, so the experiment will determine whether the suggested configuration is correct and what is the amount of admixture.

For the measurement of g factors of interest we applied the Time Dependent Perturbed Angular Distribution (TDPAD) method, which is based on measuring the perturbation of the γ anisotropy of the spin-oriented nuclear ensemble due to an externally applied magnetic field. Prior to this experiment, several TDPAD measurements on isomers produced in fragmentation reactions of the primary beam at relativistic [5] and intermediate energies [6,7] were performed. A major requirement to study the nuclear electromagnetic moments is to observe the decay of a spin-oriented ensemble. In fragmentation reactions, spin orientation of the isomers is obtained in the reaction itself and it is necessary to preserve the produced alignment to the implantation point. As the isomers are in-flight mass separated, the hyperfine interaction between the nuclear and random oriented electron spin can destroy the orientation of the nuclear ensemble. The fragments are produced fully stripped due to the high energy of the primary beam. The pick-up of electrons increases with Z of the ions for similar beam energy and decreases with the beam energy for ions with the same Z. This limits the opportunities to perform such experiments at intermediate energies of the primary beam ($E/A \sim 60 - 100$ MeV) to masses $A \leq 80$. For heavier nuclei such experiments can be done only with relativistic beams, which are available at GSI.

2 Experiment

The neutron-rich nuclei around $A \approx 130$ were produced in relativistic projectile fragmentation of a ^{136}Xe beam at $E/A = 600$ MeV on a thin 1024 mg/cm^2 Be production target. The primary beam, which had an average intensity of $2 \cdot 10^9$ ions per 10 s spill, was provided by the GSI heavy ion synchrotron (SIS). The fully-stripped ions were separated and identified with the two-stage high resolution magnetic zero-degree FRagment Separator (FRS) [8], which was operated in the standard achromatic mode. A schematic view of the set-up is shown in Figure 1.

The longitudinal momentum distribution of the fragments was measured by the position sensitive scintillator detector *Sc21* in the second focal plane of FRS (*S2*). In front of it, slits were introduced to cut the primary beam. The time of flight, measured with scintillator detectors *Sc21* and *Sc41* (see Figure 1) together with the magnetic rigidity of the beam, $B\rho$, was used to determine the mass-to-charge ratio, A/q. The ion charge Z was determined by the energy loss in the MUlti-Sampling Ionization Chamber (*MUSIC*) at the final focus. This allows the identification of the ions which reach the final focus of the FRS as shown in Figure 2. The multiwire proportional chambers, *Mw41* and *Mw42*, together with the position information from *Sc21*, were used for the precise beam tracking of each ion.

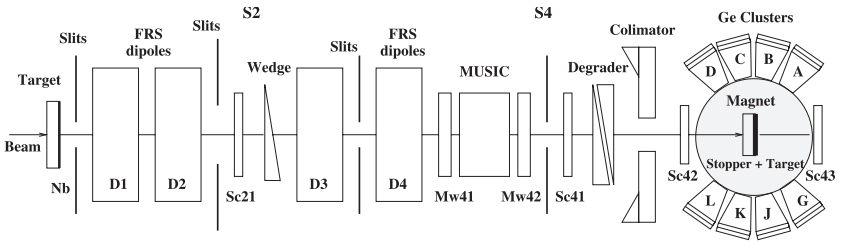

Figure **1.** Schematic view of the experimental set-up consisting of the FRS, the beam-line detectors, the γ-ray detectors and an electromagnet (see text for explanations).

The ^{127}Sn secondary beam was transported through the FRS with an energy of 300 MeV per nucleaon. At the final focal plane of FRS (*S4*) the ions were stopped by using a thick 15 mm Plexiglas degrader glued in front of a high-purity (99.998%) 2 mm annealed Copper plate which served as an implantation host. It has a cubic lattice, without electric field gradients, and provided a perturbation-free environment for the implanted ions. It was placed between the poles in the center of an electromagnet that provided a constant magnetic field $\vec{B}$ in the vertical direction. The magnet was shielded upstream with a Pb brick wall. The beam entered the magnet through a hole in the yoke with a diameter of 75 mm. Upstream a Pb collimator was built in in the Pb wall with a diameter of 70 mm. In this way, the beam spot at the secondary target position had a diameter of 70 mm. Two additional scintillator detectors, *Sc42* and *Sc43*, were placed in front and behind the catcher, which allows us to validate the implantation of the impinging ions.

The isomeric γ rays were detected with eight Cluster Ge detectors mounted in the horizontal plane perpendicular to the magnetic field. A Cluster detector consists of seven tapered hexagonal Ge crystals in a common cryostat. Each crystal can act

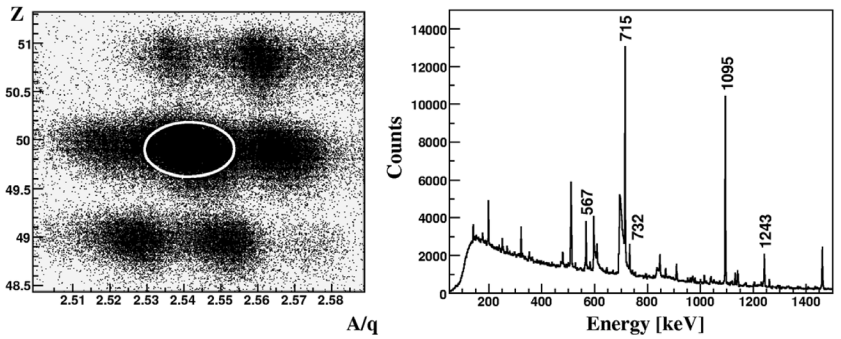

Figure **2.** Left: Typical identification plot; the ellipse indicates the gate on ^{127}Sn. The spots left and right of it correspond to ^{126}Sn and ^{128}Sn, respectively, while the upper ones are for ^{129}Sb and ^{130}Sb, and the lower ones for ^{124}In and ^{125}In. Right: Energy spectrum for ^{127}Sn gated on the identification plot. The labelled transitions belong to the decay of the $19/2^+$ isomer.

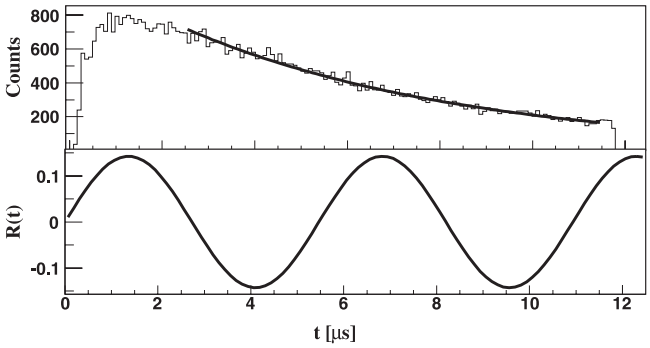

Figure **3.** Top: Time spectrum for the 1095 keV line in ^{127}Sn with the half-life of 4.5(3) μs; Bottom: Calculated $R(t)$ function assuming $g = -0.1$ and a magnetic field $B = 0.12$ T.

as a separate detector. The average distance from the stopper to the front face of the detectors was approximately 43 cm. The total γ-ray efficiency was measured by placing a calibrated ^{152}Eu source at six different positions at the catcher, covering the whole implantation spot and is approximately 2% at 1000 keV. In Figure 2 (right) an isotope gated energy spectrum is presented. There are some contaminating transitions from neighbouring Sn isotopes and background lines in the spectrum.

The nuclei of interest were identified on an event-by-event basis. Coincidences between ion signals from the FRS detectors and γ rays detected with the Ge detectors were recorded within a time window of 12 μs, provided by a common time-to-amplitude converter. In addition, signals from each crystal of the Cluster detectors were sent to an individual TDC, which opened an extra 2 μs window. This allows successive isomers to be studied, as well as to time-align the individual crystals. The fast signal from *Sc41* which was generated by an impinging ion was used to start the time measurement ($t = 0$ signal). The measured time spectrum for the $19/2^+$ isomer in ^{127}Sn is presented in the top section of Figure 3.

The magnetic field $B = 0.12$ T was chosen such that with the minimal expected g factor of $g = -0.1$ at least two periods in the $R(t)$ function occur, as demonstrated in the bottom part of Figure 3. The direction of the magnetic field was switched manually up and down every four hours during the experiment.

3 Data Analysis

Within the present experiment in total $2 \cdot 10^5$ single-hit photopeak events ($2.5 \cdot 10^5$ photopeak events in add-back mode), which belong to the γ-decay of the $19/2^+$ isomer in ^{127}Sn, were detected. In order to extract the experimental $R(t)$ function, it is necessary to apply conditions on the longitudinal momentum distribution, by selecting events which belong either to the center, or to the wing. This reduces the number of events which are used in the data analysis, as presented in Table 1. At this stage of the analysis only single-hits in each Cluster were considered.

Table **1.** Number of counts for the measured γ rays belonging to the decay of the $19/2^+$ isomer in ^{127}Sn for all detectors, and for both directions of the magnetic field.

	1095 keV	732 keV	715 keV
Center	23980	8360	33590
Wing	13700	4870	19030
Total	68100	23700	94900
Total[1]	66435	6318	58998

[1] after background subtraction

3.1 The $R(t)$ Functions

The constant magnetic field B induces rotation of the spins of the aligned nuclear ensemble around the magnetic field axis with a Larmor frequency $\omega_L = -\frac{g\mu_N B}{\hbar}$ which depends on the isomeric g-factor and applied magnetic field. The intensity of the γ decay, detected in the horizontal plane at an angle θ with respect to the beam axis is related to the angular distribution:

$$I(t,\theta,\omega_L) = I_0 e^{-\lambda t} W(t,\theta,\omega_L) \\ = I_0 e^{-\lambda t}\{1 + A_2(\gamma)B_2 P_2[(\cos(\theta - \omega_L t - \alpha))]\}. \quad (1)$$

Here $A_2(\gamma)$ is the angular distribution coefficient, depending on the details of the γ decay, B_2 is the orientation parameter, depending on the degree of alignment produced in the reaction. $P_2(\cos(\theta))$ is the 2^{nd} order Legendre Polynomial and α is the angle between the beam direction and the symmetry axis of the spin-oriented ensemble, which in this case is equal to zero, because FRS is a zero-degree fragment separator. We neglect the 4^{th} and higher order components, because they are usually about an order of magnitude smaller.

To extract the precession pattern from measured time spectra, they are combined in $R(t)$ functions for each γ transition

$$R(t,\theta,\theta',\omega_L) = \frac{I_1(t,\theta,\omega_L) - I_2(t,\theta',\omega_L)}{I_1(t,\theta,\omega_L) + I_2(t,\theta',\omega_L)}, \quad (2)$$

where I_1 stays for the time spectrum of a detector placed at an angle θ with respect to the beam, and I_2 is the time spectrum for a detector at an angle θ'. This expression does not depend on the isomeric decay constant. It has the highest amplitude for the detectors placed at 90° with respect to each other and at $\pm 45^\circ$ and $\pm 135^\circ$ with respect to the beam axis, provided that $\alpha = 0$.

$$R(t,\omega_L) = \frac{3A_2B_2}{4 + A_2B_2}\sin(2\omega_L t). \quad (3)$$

It is possible to compose an $R(t)$ using the data from the same detector but for two opposite directions of the magnetic field. For a detector placed at angle θ we obtain

$$R(t,\theta,\pm B,\omega_L) = \frac{3A_2B_2\sin(2\theta)\sin(2\omega_L t)}{4 + A_2B_2 + 3A_2B_2\cos(2\theta)\cos(2\omega_L t)}. \quad (4)$$

Using such $R(t)$ functions we eliminate some detector-related effects which can cause systematic errors.

If the specific symmetries of the set-up are considered we arrive to an expression for the $R(t)$ function identical with Eqn. (3) for the detectors at $\pm 45^\circ$ and $\pm 135^\circ$. This means that the following detector combinations are possible (see Figure 1 for the detector labels): $I_1 = (A+L)\uparrow + (D+G)\downarrow$ and $I_2 = (A+L)\downarrow + (D+G)\uparrow$, where $\uparrow$ and $\downarrow$ denotes opposite directions of the applied field. Similarly another combination of detectors can be done, but the amplitude of the $R(t)$ function will be reduced and the phase will be shifted. For example, if the detectors at $\pm 75^\circ$ and $\pm 105^\circ$ with respect to the beam direction ($\pm 30^\circ$ with respect to each other) are considered ($I_1 = (B+K)\uparrow + (C+J)\downarrow$ and $I_2 = (B+K)\downarrow + (C+J)\uparrow$), the $R(t)$ function will have almost the same phase as in Eqn. (3), but twice smaller amplitude

$$R(t,\omega_L) = \frac{3A_2B_2\sin(2\omega_L t)}{8 + 2A_2B_2 - 3\sqrt{3}A_2B_2\cos(2\omega_L t)}. \quad (5)$$

For the combination of detectors at $\pm 150^\circ$ with respect to each other, $\pm 45^\circ$ and $\pm 105^\circ$ with respect to the beam, the following time spectra can be considered: $I_1 = (A+L)\uparrow + (C+J)\downarrow$ and $I_2 = (K+B)\uparrow + (G+D)\downarrow$. The $R(t)$ function will have a phase shift and twice smaller amplitude

$$R(t,\omega_L) = \frac{3A_2B_2(\sin(2\omega_L t) + \sqrt{3}\cos(2\omega_L t))}{16 + 4A_2B_2 + 3A_2B_2(3\sin(2\omega_L t) - \sqrt{3}\cos(2\omega_L t)}. \quad (6)$$

The phase shift of the $R(t)$ function depends on the value of the g factor, while the reduction of the amplitude is fixed for each combination of detectors. This allows a simultaneous fit of all detector combinations using two fit parameters, the Larmor frequency and the amplitude of the $R(t)$ function, which is related to the orientation of the nuclear spin ensemble.

Most of the crystals of the Cluster detectors do not lie exactly in the horizontal plane, but are misaligned at a small angle ϕ. This causes an additional reduction of the amplitude. However, due to the large distance between the implantation spot and the detector faces, this effect, as well as the influence of geometric factors due to the finite dimensions of the implantation spot, can be neglected. A more elaborate analysis needs to take into consideration the implantation position of each ion, and the crystal of the first hit in a Cluster detector. Here we report results obtained only with detectors at 90° with respect to each other, at $\pm 45^\circ$ and $\pm 135^\circ$ with respect to beam axis.

3.2 Momentum Selection

In fragmentation reactions the fragments have a longitudinal momentum distribution $exp(-p^2/2\sigma^2)$, with $\sigma = \sigma_0^2 A_{fr}(A_p - A_{fr})/(A_p - 1)$, where A_p and A_{fr} are the mass numbers of the projectile and the fragment, and $\sigma_0 \approx 90$ MeV/c [9].

The alignment of the nuclear spin ensemble depends on the longitudinal momentum distribution [7]. Under alignment of the nuclear ensemble the different m substates for a given spin I, $m = -I, -I+1, ..., I$ have different population, but the $\pm m$ substates are equally populated. Positive (oblate) alignment occurs when the spin ensemble is oriented in a plane perpendicular to the beam axis, while for negative (prolate) alignment the spins are oriented perpendicularly to this plane. It is obvious that a change of the sign of the alignment will result in a change of the sign of the $R(t)$ function. Experiments at intermediate energies demonstrated that the alignment changes its magnitude and sign from the center towards the outermost wing of the momentum distribution. This effect was studied also theoretically and qualitative understanding was achieved [10]. Therefore, it is necessary to determine the position of the center and the wing to eliminate interference effects resulting from mixing of alignment. So far some measurements were done at intermediate energies and such data did not exist at relativistic energies.

The measured momentum distribution with *Sc21* is shown in the left-hand-side of Figure 4. The lower wing was cut with the $S2$ slits of the FRS (see Figure 1). During the experiment the shape of the momentum distribution gradually changed to more complicate form. The reason is that beam which hits scintillator *Sc21* was close to the maximum ($2 \cdot 10^5$ ions/s) and the properties of the scintillator deteriorated. For this reason we deduced the isomeric ratio for the $19/2^+$ isomer in ^{127}Sn as a function of the momentum distribution and used it as a criterium to define the position of the center and the outermost wing (see Figure 4, right). The isomeric ratio is expected to have a minimum in the center and maximum in the wing of momentum distribution [11].

The isomeric ratio is defined as the probability that in a reaction an isomeric state is excited

$$IR = \frac{Y}{N_{imp}FG} = \frac{N_\gamma(1+\alpha_{tot})}{\epsilon_{eff} b_\gamma N_{imp} FG}, \tag{7}$$

where N_γ is the number of counts in the peak corresponding to the transition depopulating the isomer, α_{tot} is the total conversion coefficient for this transition, b_γ is its

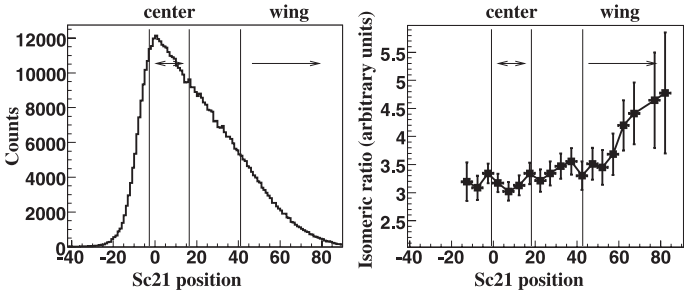

Figure **4.** Left: Longitudinal momentum distribution for ^{127}Sn measured with *Sci21*; Right: The isomeric ratio for the $19/2^+$ isomer in ^{127}Sn as a function of momentum distribution. The positions of center and wing are indicated with vertical lines.

absolute branching ratio, ϵ_{eff} is the efficiency correction and N_{imp} is the number of implanted ions of the isotope of interest. F and G are the correction factors for the inflight isomer decay and the finite detection time of the γ ray, respectively. The isomeric ratio plotted in Figure 4 is the average for the most intense transitions in ^{127}Sn, without corrections which do not depend on momentum distribution. At this stage of the analysis it is enough to determine the relative, not the absolute values for the isomeric ratio.

4 Results and Discussion

The $R(t)$ functions of the 1095 keV and 715 keV γ rays and for different cuts of the longitudinal momentum distribution are presented in Figure 5. The amplitude of the $R(t)$ function, which is sorted for the sum of the time spectra of the 1095 keV E2 and 732 keV M2 transition for the center of the momentum distribution (see the middle section of Figure 5), is very small and has an opposite phase compared to the $R(t)$ function for the outermost wing (see the upper section of Figure 5). This indicates a sign change of the alignment of the nuclear spin ensemble between the center and the wing of the momentum distribution.

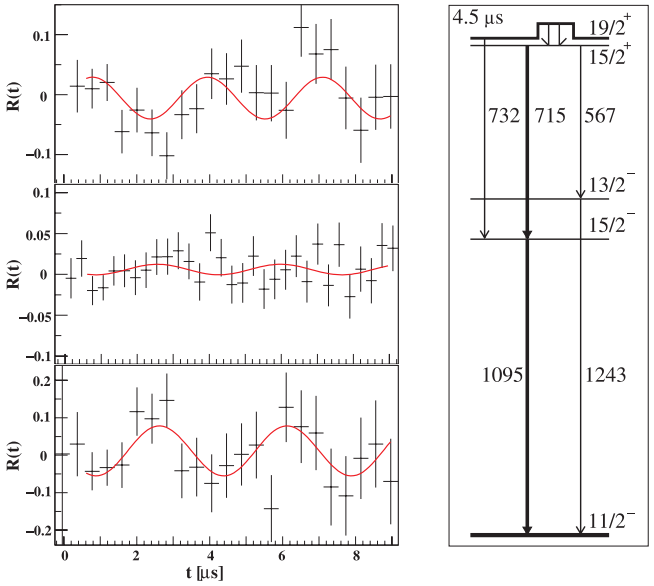

Figure **5.** Left: (up) $R(t)$ function for the 1095 keV and 732 keV transitions at the wing of the momentum distribution; (middle) $R(t)$ function for 1095 keV and 732 keV transitions at the center of the momentum distribution; (down) $R(t)$ function for 715 keV transition at the wing of the momentum distribution. Right: Partial level scheme of ^{127}Sn, revealing the decay of the $19/2^+$ isomer [2].

The $R(t)$ function for the 715 keV transition was sorted for the outmost wing of the momentum distribution (see the lower section of Figure 5). It display opposite phase, compared to the $R(t)$ function for the 1095 keV transition, which is not in agreement with the published level scheme [2]. According to the published spin and parities, the 715 keV transition should have E1 multipolarity. In such a case its angular distribution coefficient would be $A_2 = -0.4$, which is similar to the values of the coefficients for the 1095 keV E2 transition, $A_2 = -0.39$, and the 732 keV M2 transition, $A_2 = -0.37$ [12].

Fits of the $R(t)$ functions are displayed in Figure 5. The obtained absolute values of the g factor, $|g| \approx 0.16$ are in agreement with the theoretical expectations based on the empirical g factors and on large-scale shell model calculations. These results will be discussed elsewhere [13].

For the $R(t)$ function of the 715 keV transition $\sim 10^4$ photopeak events were used in the data analysis, which provides the lower limit for such experiments.

5 Conclusions

First results from the g-RISING campaign for the g factor of the $19/2^+$ isomer in ^{127}Sn from relativistic fragmentation demonstrate that significant alignment ($\sim$10%) is observed in the outermost wing of the momentum distribution. The results indicate that a sign change of the alignment takes place between the center and the wing. The present experiment provides a benchmark (in terms of intensity of the isomer beam and number of detected γ rays) for further determinations of electromagnetic moments of isomers in nuclei yet farther away from stability.

Acknowledgments

This work was supported in part by the EC EURONS RII3-CT-2004-506065 project and the Bulgarian National Science Fund grant VUF06/05.

References

1. H. J. Wollersheim *et al.*, *Nucl. Instr. Meth. Phys. Res. A* **537**, 637 (2005); `www-aix.gsi.de/~wolle/EB\_at\_GSI/FRS-WORKING/main.html`
2. J. A. Pinston *et al.*, *Phys. Rev. C* **61**, 024312 (2000).
3. J. A. Pinston and J. Genevey, *J. Phys. G* **30**, R57 (2004).
4. P. Raghavan, *Atomic Data and Nuclear Data Tables* **42**, 189 (1989).
5. W. D. Schmidt-Ott *et al.*, *Z. Phys. A* **350**, 215 (1994).
6. G. Georgiev *et al.*, *J. Phys. G* **28**, 2993-3006 (2002).
7. I. Matea *et al.*, *Phys. Rev. Lett.* **93** 142503, (2004).
8. H. Geissel *et al.*, *Nucl. Instr. Meth. B* **70**, 286 (1992).
9. A. S. Goldhaber, *Phys Lett B* **53**, 306 (1974).

10. N. Coulier *et al.*, *Phys. Rev. C* **63**, 054605 (2001).
11. J. M. Daugas *et al.*, *Phys. Rev. C* **63**, 064609 (2001).
12. T. Yamazaki, *Nuclear Data A* **3**, 1 (1967).
13. L. Atanasova *et al.*, in preparation (2006).